ISSN 1062-8738, Bulletin of the Russian Academy of Sciences: Physics, 2020, Vol. 84, No. 4, pp. 500–504. © Allerton Press, Inc., 2020.

Detection of the Low Energy Recoil ^{3}He in the Reaction ^{2}H(^{8}He,^{3}He)^{7}H

I. A. Muzalevskii[a, b, *], V. Chudoba[a, b], S. G. Belogurov[a, d], A. A. Bezbakh[a, b], D. Biare[a], A. S. Fomichev[a, e], S. A. Krupko[a, c], E. M. Gazeeva[a], M. S. Golovkov[a, e], A. V. Gorshkov[a], L. V. Grigorenko[a, d, f], G. Kaminski[a, g], O. Kiselev[h], D. A. Kostyleva[h, i], M. Yu. Kozlov[j], B. Mauyey[a, n], I. Mukha[h], E. Yu. Nikolskii[a, f], Yu. L. Parfenova[a], W. Piatek[a, g], A. M. Quynh[a, k], V. N. Schetinin[j], A. Serikov[a], S. I. Sidorchuk[a], P. G. Sharov[a, b], R. S. Slepnev[a], S. V. Stepantsov[a], A. Swiercz[a, l], P. Szymkiewicz[a, l], G. M. Ter-Akopian[a, e], R. Wolski[a, m], and B. Zalewski[a, g]

[a] *Flerov Laboratory of Nuclear Reactions, Joint Institute for Nuclear Research, Dubna, Moscow oblast 141980 Russia*
[b] *Institute of Physics, Silesian University in Opava, Opava, 74601 Czech Republic*
[c] *Institute for Theoretical and Experimental Physics, National Research Centre "Kurchatov Institute," Moscow, 117218 Russia*
[d] *National Research Nuclear University "MEPhI", Moscow, 115409 Russia*
[e] *Dubna State University, Dubna, Moscow oblast 141982 Russia*
[f] *National Research Centre "Kurchatov Institute," Moscow, 123182 Russia*
[g] *Heavy Ion Laboratory, University of Warsaw, Warsaw, 02-093 Poland*
[h] *GSI Helmholtz Center for Heavy Ion Research, Darmstadt, 64291 Germany*
[i] *II. Institute of Physics, Justus Liebig University, Giessen, 35392 Germany*
[j] *Laboratory of Information Technologies, Joint Institute for Nuclear Research, Dubna, Moscow oblast 141980 Russia*
[k] *Nuclear Research Institute, Dalat, 670000 Vietnam*
[l] *Faculty of Physics and Applied Computer Science, AGH University of Science and Technology, Krakow, 30-059 Poland*
[m] *Institute of Nuclear Physics, Polish Academy of Sciences, Krakow, 31342 Poland*
[n] *Institute of Nuclear Physics, Almaty, 050032 Kazakhstan*
**e-mail: muzalevsky@jinr.ru*

Received October 30, 2019; revised November 25, 2019; accepted December 27, 2019

Abstract—Investigation of the ^{7}H-system in the experiment conducted at the fragment separator ACCULINNA-2 in the ^{8}He(^{2}H,^{3}He)^{7}H reaction requires to detect the recoil ^{3}He ions with energy down to 6 MeV. For this purpose two $\Delta E-E$ particle telescopes are used, with each telescope having in front a thin (20-μm) Si strip detector (ΔE–SSD). The maps of thickness heterogeneity of the thin detectors were determined by measuring the energy losses of the ^{226}Ra α-particles. The adopted thickness normalization method provides a good identification of the ^{3}He nuclei being recorded in the presence of a high ^{4}He background. Two approaches were used for calculating the energy losses of the identified ^{3}He and ^{4}He reaction ejectiles and reconstructing their energy values available at the exit from the deuterium target. The developed techniques were applied for the ^{7}H missing-mass reconstruction.

DOI: 10.3103/S106287382004019X

INTRODUCTION

Investigation of the nuclear systems in the vicinity of the drip lines is one of the main objects of interest in the modern nuclear physics. Although this task is very complicated, the development of high-precision experimental techniques, and particle detectors, allows one to penetrate beyond the nuclear-stability boundary. The study of ^{7}H, the nucleus with the largest accessible mass to the charge ratio is an example of this progress. Although the assumption of the existence of the ^{7}H was made more than 50 years ago [1], few attempts of search for the quasi-stable or long-living ^{7}H [2–4] were undertaken but all of them were either unsuccessful, or provided only the upper limits for the studied reaction cross sections or the ^{7}H lifetime.

It is suggested that the four neutrons in the ^{7}H system occupy the same orbits as in ^{8}He [5]. That is why it is reasonable to suppose that the most promising way for production of the ^{7}H system is the proton-transfer

reaction from the ^{8}He core. This approach was employed in several experiments using the ^{2}H(^{8}He,^{3}He)^{7}H reaction [5–7]. All of them gave similar results, but the insufficient energy resolution and the low statistics of the measured data did not allow the authors to make definite conclusions about the excitation spectrum of this nucleus.

One of the most important tasks for the last study of the ^{7}H states populated in the ^{8}He(^{2}H,^{3}He)^{7}H reaction [8] was the proper selection of the reaction channel. The ^{7}H missing mass spectrum was reconstructed from energy and emission angle of the ^{3}He ejectile nuclei registered in coincidence with the tritons (^{3}H) originating from the decay of ^{7}H. To obtain valuable results, a reliable particle identification (PID) and a high-precision reconstruction of the ^{3}He momenta in the interaction point was essential.

In the specific case of the ^{8}He(^{2}H,^{3}He)^{7}H reaction the employment of the $\Delta E-E$ PID method for the ^{3}He recoil identification requires to use a thin silicon strip detector. A wafer-etching process is usually employed for the production of such detectors, which fact forces us to take care of measuring individual characteristics of each detector [9]. We used two very thin ΔE–SSDs, namely W1 (SS)-20 Type 2M, produced by Micron Semiconductor Ltd [10].

In this work, we report the developed techniques for the ^{3}He identification and the reconstruction of its kinetic energy obtained at the exit from the target. The developed techniques were applied for the ^{7}H missing-mass reconstruction [8].

SEARCH FOR ^{7}H

The differential cross section for the binary ^{8}He(^{2}H,^{3}He)^{7}H reaction was calculated by the coupled channel method [11]. Furthermore, the kinematics of the binary reaction, assuming the isotropic 5-body decay of the ^{7}H nucleus, was calculated within the ExpertRoot framework [12]. The results presented in the Fig. 1 indicate the ranges of the energies and emission angles of the reaction products expected for the ^{8}He beam energy 26 MeV per nucleon.

It is predicted that for the ^{7}H excitation energy less than 6 MeV one should expect the kinetic energy of the recoil ^{3}He ion in the interaction point lies in a range between 10 and 20 MeV. Tritons emitted further in the ^{7}H decay (not shown in Fig. 1) have kinetic energy 60 to 90 MeV and are emitted at angles less than 9° in the laboratory system.

The ^{8}He(^{2}H,^{3}He)^{7}H reaction was studied in the experiment conducted at the Flerov Laboratory of Nuclear Reactions. A beam of the ^{8}He with energy ~26 A MeV was produced by the ACCULINNA-2 fragment separator [13] and focused on the 4-mm thick target cell filled with ^{2}H gas at the temperature of

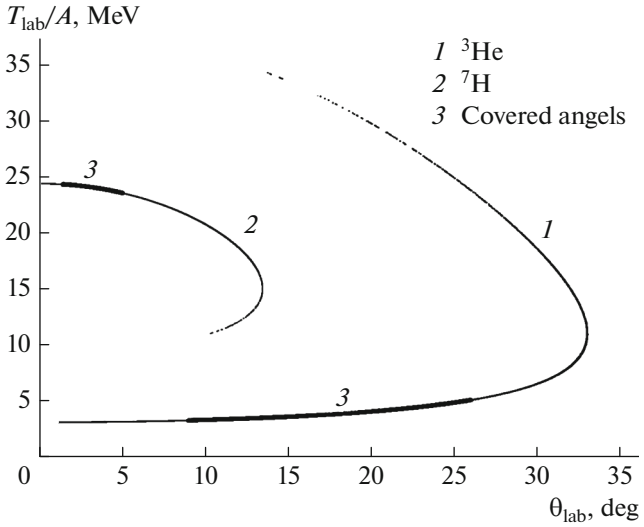

Fig. 1. Dependence of the kinetic energy per nucleon of the ^{7}H and recoil ^{3}He on the angle in the laboratory frame of reference. The curve *1* and curve *2* relates to the ^{7}H and ^{3}He, respectively. The curve *3* refers to the angle areas covered by the detectors.

27 K and pressure 1150 mbar. The target cell was supplied with the 6 μm steel entrance and exit windows. For the for thermal insulation this cell was equipped with two 3.5 μm Mylar windows. The pressure of the ^{2}H inside the target cell caused the inflation of steel windows, that is why the target was shaped in the lenticular form with the maximum thickness of ~6 mm.

Taking into account the average energy losses in the material of the different layers of the target, one should expect to measure the recoil ^{3}He with energies down to 6 MeV. We used standard PID method for the ^{3}He and ^{3}H detection, based on the comparison the energy losses in first layer of the telescope (ΔE) and the remaining energy in the second layer (E). Coincidence of the ^{3}He and ^{3}H is considered as the main indication of the ^{7}H population.

Two $\Delta E-E$ telescopes were used for the detection of the recoil ^{3}He nuclei and one telescope placed at zero-angle in respect to the beam axis was used to detect the tritons emitted from ^{7}H. The triton telescope was constructed of the 1.5-mm thick double-side SSD and an array of 16 CsI(Tl) crystals. Two identical ^{3}He telescopes positioned downstream on the two sides from the beam axis and covered angular range 9°–27° in the laboratory system. Each of these telescopes consisted of 3 silicon detectors. A 20-μm thick Si ΔE–SSD (50 × 50 mm^2, 16 strips) occupied the front position in the telescope, and the pair of identical 1-mm thick (both 60 × 60 mm^2, 16 strips) SSDs were placed on the second and third positions. In order to track the particles with such telescopes, the

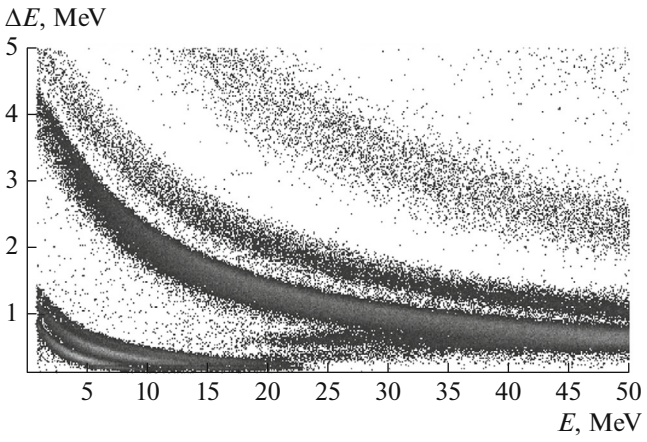

Fig. 2. $\Delta E-E$ PID plot for all strips of one ^{3}He telescope before thickness normalization. Vertical and horizontal axes show the energy deposit in millielectronvolts in the 20-μm thick (ΔE) and 1-mm thick (E) detector, respectively. One may see that only isotopes with different charge ($Z = 1$, $Z = 2$, $Z = 3$) can be distinguished.

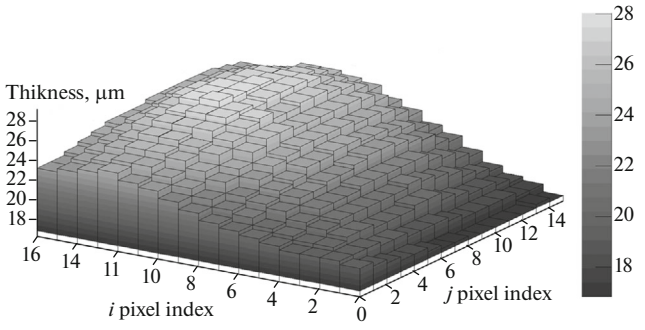

Fig. 3. The thickness map for one of the 20-μm thick detector. Vertical axis shows the calculated pixels' thickness in micrometers. Pixel indexes i and j represent the strips fired in the 20-μm thick and 1-mm thick detector, respectively. Unlike index i, which takes values 1–16, index j accepts values from 1 to 15 which is due to the fact that the first strip of the second SSD layer was shaded by the housing frame of the 20-μm thick detector.

strips of the first (20 μm) and the second detectors were set to be perpendicular to each other. The third SSD was used as a veto detector for to eliminate signals coming from the particles penetrating the second layer. These were mostly the high-energy ^{4}He and ^{8}He ions.

SILICON TELESCOPES FOR THE ^{3}He DETECTION

For the determination of the dead layers on the surfaces of all silicon detectors, and for their calibration defining the dependence of the signal value on the energy deposit made by the detected particles, the multiple-energy α-source ^{226}Ra was used. We assumed the linear dependence of the Si detector response on the energy deposit and achieved the energy resolution of all silicon detectors being just about 70 keV (FWHM).

The first attempt of the ^{3}He identification by means of the (ΔE vs. E) PID plot obtained in the experiment was not satisfactory. In Fig. 2 the PID plot from one of the ^{3}He telescopes is presented. One can see that the hydrogen isotopes can be distinguished from the helium group, but the ^{3}He cannot be observed being mixed up with ^{4}He.

In order to achieve reliable ^{3}He identification the thickness inhomogeneity of the 20-μm thick detectors has to be correctly taken into account. The thickness inhomogeneity maps were determined as follows. We call a pixel the part of the ith strip of the first-layer detector corresponding to the jth strip (oriented orthogonally) of the second-layer detector. Thus each 20-μm thick detector has $I \times j$ pixels in total.

For measuring the thickness of each pixel the both ^{3}He telescopes were irradiated by α-particles emitted by ^{226}Ra, placed at a distance of 35 cm from the first detector plane, so that the α-particles hit the central pixels at approximately 90°. The energy loss in the 20-μm detector as a function of the fired strips numbers in the first and the second layer detector was derived from the shift of the peaks in the 1-mm detector compared to measurements made without the 20-μm detector.

According to the LISE++ [14], α-particles with initial energy ~7.68 MeV penetrate ~46 μm of silicon, which suggests that the Bragg peak locates deeply in the sensitive area of the second layer SSD. It was observed that among all the particles emitted by the source only these α-particles with the highest energy could always penetrate the 20-μm detector and the dead layer of second SSD giving in this SSD the signals with amplitude above the noise threshold. That is why only these signals were used for the thickness analysis.

The obtained values of the energy losses were converted into the thickness using parameterization from GEANT4 EMStandard_opt0 sub-package [15].

The thickness distribution of one of the 20-μm thick $\Delta E-$SSD is shown in Fig. 3. Although the number of strips of the first and the second layer SSDs is 16, one may see that the obtained thickness map consists of less than 16 × 16 pixels. It is caused by the shading of the second layer SSD by the supporting frame of the 20-μm thick detector. The obtained thickness distribution turned out to be quite non-uniform. Although it was declared by the manufacturer that such detectors have thickness variation not more than 2 μm from the nominal value (20 μm), one can see that the investigated detector does not meet this criterion. In order to check the results, the thickness non-uni-

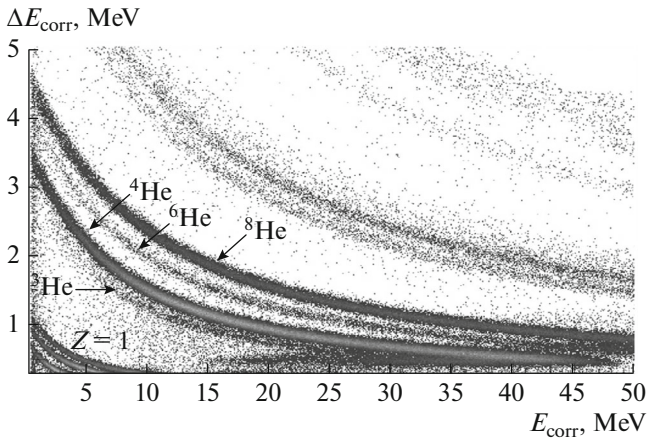

Fig. 4. ΔE–E PID plot for all strips of the ^{3}He telescope after thickness normalization. Vertical and horizontal axes show the energy deposits in two SSDs with the thickness correction as described in the text. All isotopes are nicely separated from each other; ^{3}He nuclei can be also observed.

formity was also verified with the LISE++ energy loss parameterization. The thickness maps obtained by both methods are consistent within less than 1 μm.

The thickness maps were used to improve the isotope separation obtained in the ΔE–E identification plot. Note that poor statistics did not allow us to build the identification plots individually for each pixel. Under the assumption of the small thicknesses, the energy loss of a particle per unit path ($\Delta E/\Delta X$) can be considered as constant. The energy losses occuring for different ΔX are proportionally related, which fact was used for the ΔE normalization performed in the following way:

$$\frac{\Delta E_k}{\Delta E_{corr}} = \frac{X_k}{\overline{X}},$$

where X_k and ΔE_k represent the thickness of the kth pixel and the energy loss in its sensitive area; ΔE_{corr} is the corrected energy; $\overline{X}$ is the normalization thickness value (20 μm in our case). An amendment to the ΔE_k was used to correct the energy deposit in the second layer SSD:

$$E_{corr} = E_k + \Delta E_k - \Delta E_{corr},$$

where ΔE_k and ΔE_{corr} denote, respectively, the energy deposits in the 20-μm ΔE–SSD obtained before and after correction.

The PID plot obtained by the above described correction method is presented in Fig. 4, where the same experimental data as used in Fig. 2 were processed. One may observe that the loci of ^{3}He and ^{4}He are clearly distinguishable, i.e. the developed method provides reliable ^{3}He identification.

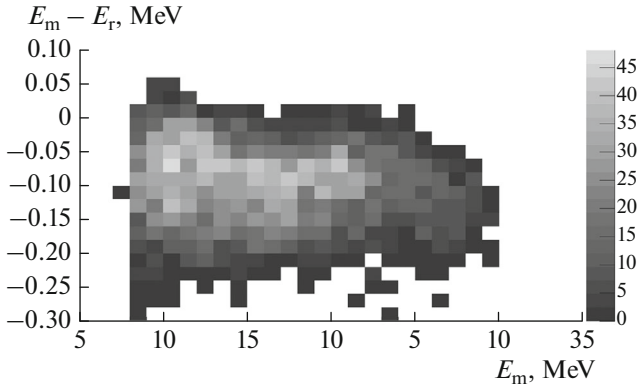

Fig. 5. The ^{3}He energy difference $E_m - E_r$ correlation, calculated by two methods, with the total energy of the ^{3}He (E_m). See text for detail.

^{3}He ENERGY RECONSTRUCTION

The energy of the ^{3}He at the interaction point was calculated using the G4EMCalculator class accessed via the ExpertRoot framework. It is essential that the same energy-loss parameterization was used both for the determination of the thickness map and for the ^{3}He energy calculation. For this reconstruction the passive parts of the target and dead layers of the detectors were taken into account in going consecutively along the particle trajectory. The angle of the ^{3}He emission was also taken into account. As an additional cross check, we used two methods for the ^{3}He energy reconstruction in the interaction point.

In the first method, the measured kinetic energy of the ^{3}He in the interaction point (E_m) was taken as a sum of the energy deposits in the 1-mm thick SSD (E), in the 20-μm thick detector and added to this were the calculated average energy losses in the target and the detectors' dead layers. In the second method, the reconstructed kinetic energy of the ^{3}He in the interaction point (E_r)included only the sum of the energy measured in the second, 1-mm SSD and the calculated average energy losses in the entire thickness of the corresponding pixel of the front, 20-μm ΔE–SSD and target volumes. The $E_m - E_r$ difference is presented in the Fig. 5 as a function of the reconstructed ^{3}He energy in the interaction point. One can see that the energy E_r, obtained by the second method is systematically higher than E_m. This fact can be understood because, in the second method, the larger specific energy losses calculated for the smaller energy released in the second detector are extrapolated to the lager range. The absolute value of the difference $E_m - E_r$ slightly increases with the ^{3}He energy but it is still comparable with the SSD energy resolution (70 keV).

CONCLUSIONS

The study of the ^{7}H-system obtained in the ^{8}He(^{2}H,^{3}He)^{7}H reaction at beam energy 26 MeV per nucleon requires to detect the ^{3}He recoil nuclei characterized by a rather low kinetic energy. This task was realized by the use of very thin (~20 μm) ΔE–SSDs, taken as the first layer of the silicon detector telescopes. However, in such case one should take care of their thickness uniformity as far as the lack of the statistics does not allow to consider the spectra obtained separately from the numerous pixels. We have studied the thickness distribution of the 20-μm thick SSD. The developed method is based on the measured energy losses of the α-particles with the initial energy ~7.68 MeV emitted from the ^{226}Ra source passing through the detectors volume. Algorithm of the thickness calculations is based on the ExpertRoot methods. It was found that the thickness varies up to 8 μm over the whole sensitive area of the 20-μm ΔE–SSD. Such correction allows to improve the accumulated PID plot and to carry out the ^{3}He identification.

The ^{3}He energy in the interaction point was reconstructed by the two methods giving results which were in good agreement with each other. The developed techniques were applied to the reconstruction of the ^{7}H missing-mass spectrum measured in the ^{8}He(^{2}H,^{3}He)^{7}H reaction [8]. This achievement gives us the confidence for the employment of the 20-μm thick ΔE–SSDs for the particle identification in the future experiments.

FUNDING

This work was partly supported by the Russian Science Foundation (project no. 17-12-01367) and MEYS Project Czech Republic (grant LM2015049).

REFERENCES

1. Baz, A.I., Goldansky, V.I., Goldberg, V.Z., and Zeldovich, Ya.B., *Legkie i srednie yadra vblizi granitsy stabil'nosti* (Light and Intermediate Nuclei Near the Borders of Nucleon Stability), Moscow: Nauka, 1972.
2. Seth, K.K., *CERN Report*, Geneva, no. 81-09-655, 1981, vol. 1, p. 655.
3. Evseev, V.S., Kurbatov, V.S., Sidorov, V.M., et al., *Nucl. Phys. A*, 1981, vol. 352, p. 379.
4. Golovkov, M.S., Grigorenko, L.V., Fomichev, A.S., et al., *Phys. Lett. B*, 2004, vol. 588, p. 163.
5. Korsheninnikov, A., Nikolskii, E., Kuzmin, E., et al., *Phys. Rev. Lett.*, 2003, vol. 90, 082501.
6. Nikolskii, E., Korsheninnikov, A., Otsu, H., et al., *Phys. Rev. C*, 2010, vol. 81, 064606.
7. Ter-Akopian, G.M., Fomichev, A.S., Golovkov, M.S., et al., *Eur. Phys. J. Spec. Top.*, 2007, vol. 150, p. 61.
8. Bezbakh, A.A., Chudoba, V., Krupko, S.A., et al., arXiv: 1906.07818 [nucl-ex]. Accessed August 15, 2019.
9. Liu, Q., Ye, Y., Li, Zh., et al., *Nucl. Instrum. Methods Phys. Res., Sect. A*, 2018, vol. 897, p. 100.
10. Micron Semiconductor. http://www.micronsemiconductor.co.uk/.
11. Fresco: Coupled Reaction Channels Calculations. https://www.fresco.org.uk/. Accessed August 15, 2019.
12. ExpertRoot 03. http://er.jinr.ru/. Accessed August 15, 2019.
13. Gorshkov, A.V., Belogurov, S.G., Bezbakh, A.A., et al., *Eurasian J. Phys. Funct. Mater.*, 2019, vol. 3, p. 46.
14. Tarasov, O.B. and Bazin, D., *Nucl. Instrum. Methods Phys. Res., Sect. B*, 2008, vol. 266, p. 4557.
15. GEANT4: A Simulation Toolkit. https://geant4.web.cern.ch/. Accessed August 15, 2019.